RESEARCH ARTICLE

NANO · MICRO small
www.small-journal.com

Peacock-Inspired Janus Structural Color Materials for Multi-Level Encryption and Anti-Counterfeiting

*Lulu Chen, Huateng Li, Yaoxia Li, Qilin Guo, Yuming Zang, Mengjing Zhu, Ziqiang Tian, Jia Guo, and Changchun Wang**

The existence of different miraculous structural colors in nature inspires us to continuously create new techniques, however, limitations in existing fabrication techniques, including low efficiency, small area, and imprecise structure control, have impeded their real applications. Mimicking the multi-level structure of peacock feathers, a one-step strategy is developed to efficiently manufacture the Janus structural color materials (JSCMs). Using the surface tension-regulated self-assembly of SiO_2 nanoparticles in polyethylene glycol (PEG) solution under 80 °C, the manufacturing process can be completed in a matter of minutes, which greatly improves the efficiency of photonic crystal preparation. The front and back of JSCMs contain photonic crystal (PC) and photonic glass (PG) structures, respectively. The arrangement of SiO_2 nanoparticles on the PC side is highly ordered, producing a bright iridescent color. In contrast, the order degree of nanoparticles on the PG side is low, resulting in a muted color with less angular dependence. Adjusting the molecular weight of PEG can modulate the driving force of the assembly, allowing control over the spatial position of the PC and PG domain within the film. The Janus structure also can control the fluorescence intensity of organic dyes in the film to produce diverse optical signals with great potential for multi-level information encryption and anti-counterfeiting.

1. Introduction

Structural color was first documented over 350 years ago by Robert Hooke and Isaac Newton.[1] Unlike the colors produced by dyes and pigments, structural color arises from the interaction of light with microscopic structures, resulting in vivid, stable, and non-toxic colors. Examples of structural color are common in nature, from bird feathers and butterfly scales to insect exoskeletons.[2] Research on these natural systems has inspired the development of artificial structural color materials, driving their visual applications in various fields such as optoelectronics[3] and sensing.[4]

L. Chen, H. Li, Y. Li, Q. Guo, Y. Zang, M. Zhu, Z. Tian, J. Guo, C. Wang
State Key Laboratory of Molecular Engineering of Polymers
Department of Macromolecular Science and Laboratory of Advanced Materials
Fudan University
Shanghai 200433, P.R. China
E-mail: ccwang@fudan.edu.cn

The ORCID identification number(s) for the author(s) of this article can be found under https://doi.org/10.1002/smll.202500024

DOI: 10.1002/smll.202500024

Currently, various "top–down" and "bottom–up" methods can precisely fabricate micro-nano structures to produce structural colors.[5] However, current fabrication techniques can only produce one type of ordered micro-nano structure, which typically results in a single corresponding structural color. In contrast, many animals own multiple skin structures with various structural colors.[6] For instance, male green peafowls (*Pavo muticus*) have densely packed melanin rods in the barbs of their tail feathers.[7] When the peafowl displays its tail, the front of the feathers shows vivid, metallic-like colors to attract females, while the back shows muted brown tones to avoid predators. The bright front-side coloration results from the photonic crystal (PC) structure[8] formed by the highly long-range ordered melanin rods, while the brownish back feathers have a more irregular lattice structure to conduct the photonic glass (PG) structure,[9] showing low angle-dependent color changes. This unique structure forms during peacock growth, naturally achieving structural heterogeneity and hierarchy. Generally, to achieve similar complexity, artificial structural color materials often require multiple steps to construct such structure within a single material, especially in a very thin film. Therefore, it is crucial to develop an efficient one-step method that can simultaneously generate diverse micro-nano structures to produce multiple structural colors.

Surface tension always played a crucial role in material design, providing an original power for precise structure control. By regulating the interface tension, material properties can be finely tuned in a non-invasive manner, preserving the overall integrity of the material.[10] This kind of manipulation for precise control of material structure and function at the micro-nano scale has been widely applied in coating technologies, microfluidic systems, flexible electronics, and biomedical devices.[11] Modulating surface tension is effective for designing multifunctional materials, especially for dynamic adjustment of material structures.[12] It also holds significant potential for designing structural color materials.

Inspired by the microstructure of peacock feathers, we propose a new strategy to construct Janus structural color materials (JSCMs) through surface tension-regulated self-assembly of silica nanoparticles. This approach utilizes a ternary system

of water, polyethylene glycol (PEG), and SiO_2 nanoparticles. By increasing the evaporating temperature to 80 °C, the available self-assembly time for the SiO_2 nanoparticles was significantly shortened to several minutes. As a result, only part of the SiO_2 nanoparticles formed a highly ordered structure while the rest remain less organized, resulting in a material with both long-range ordered and short-range ordered domains. The long-range ordered SiO_2 nanoparticles form a PC structure, displaying angle-dependent iridescent colors, while the short-range ordered nanoparticles form a PG structure, exhibiting structural colors with less angle-dependence. By varying the PEG molecular weight, the competition between PEG and SiO_2 nanoparticles for minimizing surface tension controls the vertical distribution of SiO_2 nanoparticles during self-assembly. This method allows for tuning of the spatial positioning of PC and PG regions within the material. The resulting material displays colors similar to peacock tail feathers, exhibiting different types of structural colors on the front and back sides. Further, by adding fluorescent molecules in the film, we leverage the differences in the photonic bandgap and quasi-photonic bandgap to achieve varied fluorescence intensities, which provides the material with multi-level optical signals, making it promising for anti-counterfeiting and information encryption.

2. Results and Discussion

2.1. Fabrication and Properties of Peacock-Inspired JSCMs

When viewed from different angles, the feathers of male blue peacocks (Figure S1A–C, Supporting Information), including eye feathers, plume feathers, and neck feathers, display a bright structural color with a metallic sheen, which changes with the viewing angle. However, when you observe the back side of the feathers, a softer color can be seen and it is almost unaffected by changes in angle. Microstructural analysis (Figure S1D, Supporting Information) reveals that each feather branch consists of two symmetrical barbules, with distinct colors on the front and back sides. This color difference arises from variations in the regularity of the microscopic structures. On the front, the rods are densely packed in a highly ordered photonic crystal structure. On the back, the rods are arranged in a more irregular way. The contrast between the front and back colors not only gives different colors to the peacock's fan-shaped tail (**Figure** 1A) but also provides protection during courtship displays.

Inspired by this structure, where the front and back sides of the same feather display different colors, we design SiO_2 nanoparticles as building blocks and PEG as the filling matrix to construct 3D photonic films (Figure 1B). Using a simple one-step evaporation method, we fabricate JSCMs with one side forming a highly ordered PC and the other side forming a PG. Interestingly, for the PEG-600 and PEG-800 systems, the PC side is on the surface (the side exposed to air) and the PG side at the bottom (the side in contact with the glass dish), while the PG side is on the surface and PC side is at the bottom for the PEG-1000 to PEG-4000 system. Due to the differences in microstructure between the surface and bottom, the film reflects white light differently, resulting in distinct colors (Figure S2, Supporting Information).

To enhance contrast and more clearly demonstrate the differences between the surface and bottom sides of the JSCMs, black pigment was added during the experiment (Figure S3, Supporting Information), and 2 wt.% identified as the optimal doping ratio. As the viewing angle changes from 0° to 60° (Figure 1C), the PC-side color of JSCM shifts from bright green to bright purple, while the PG-side color transitions from dark green to dark blue. The CIE chromaticity diagram clearly shows that the PC side (Figure S4A, Supporting Information) is positioned near the edge of the diagram, exhibiting bright colors with high saturation and wider color changes at each 10° increment. In contrast, the PG side (Figure S4B, Supporting Information) is near the center of the diagram, with softer colors and lower saturation, showing less color changes with each 10° increment. Reflectance spectra (Figure 1D,E) reveal a gradual blue shift in the reflection peaks as the angle increases. The reflection peak of the PC side shifts from 526 to 405 nm, while the PG side shifts from 527 to 459 nm, the PG side showing a smaller shift compared to the PC side. The small color change with the angle exhibited by the PG side is due to the quasi-ordered structure.[13] Additionally, the full width at half maximum (FWHM) of the reflection peaks for the PC side is narrower, all below 20 nm, whereas the PG side exhibits wider FWHM values, ≈80 nm (Figure 1F).

The differences in color and reflection peaks between the PC and PG domains stem from their distinct structures. As shown in Figure 1G,H and Figures S5,S6 (Supporting Information), the SiO_2 nanoparticles on the PC side are arranged in a highly ordered and periodic structure, while on the PG side, the long-range order is significantly reduced compared to the PC side. Furthermore, PEG-800 and PEG-1000 are chosen as representative materials to construct two types of JSCMs, which clearly illustrate the structural distinction between the surface and bottom sides (Figure S7, Supporting Information).

The structure of the JSCMs is also confirmed using Ultra-Small Angle X-ray Scattering (USAXS). The as-prepared material is placed on a rotatable sample stage (Figure 1I; Figure S8, Supporting Information), and we examine the structures of two types of JSCMs severally composed of PEG-800 and PEG-1000. As shown in Figure 1J, when $\theta = 0°$, the JSCMs are perpendicular to the X-ray beam, and the signal indicated the overall structure of the material. The 2D USAXS patterns for both types of JSCMs display multiple scattering rings, indicating a uniform distribution of silica nanoparticles with a certain degree of order. To investigate the structure of different sides of the material, we rotate the sample stage to +85° and −95° for a grazing incidence test. For the JSCM composed of PEG-800, a distinct hexagonal diffraction pattern appears at $\theta = 85°$ (rotate clockwise), indicating a highly ordered arrangement of SiO_2 nanoparticles. In contrast, at $\theta = -95°$ (rotate anticlockwise), the diffraction pattern shows multiple scattering rings, suggesting a decrease of ordering. A similar phenomenon is observed for the JSCM composed of PEG-1000, with the difference being that the diffraction spots appear at $\theta = -95°$. This difference comes from their different microstructure.

2.2. Formation Mechanism of JSCMs

The electrostatic repulsion between silica nanoparticles is the basic condition for the formation of an ordered structure in

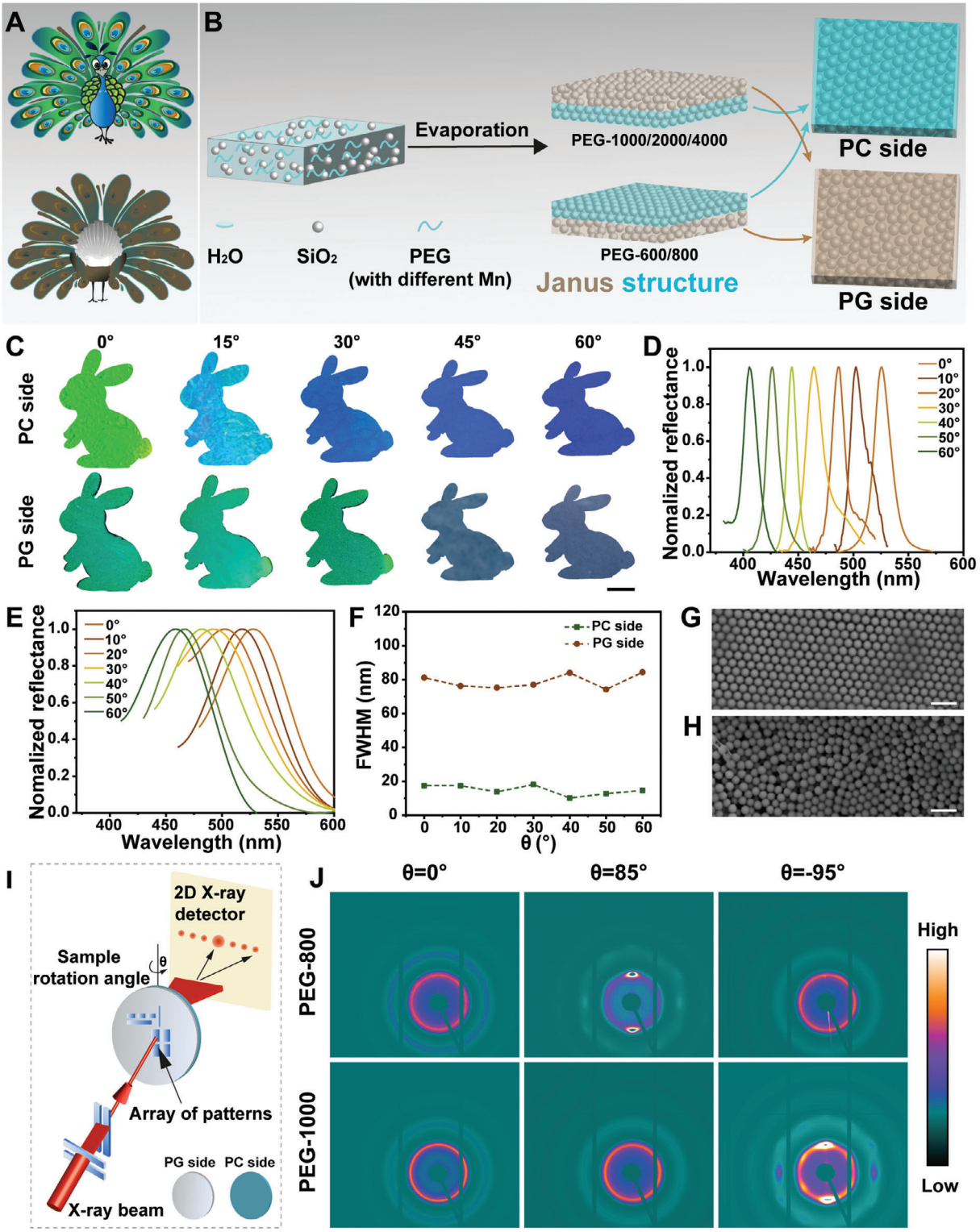

Figure 1. Design and characterization of Janus structural color materials (JSCMs) inspired by peacock feathers. A) Schematic diagram of the structural color on both sides of peacock feathers (The top is the front-side color, and the bottom is the back-side color). B) Scheme of the one-step fabrication of JSCMs. C) Digital photos, D,E) reflection spectra and F) full width at half maximum (FWHM) of reflection spectra of PC side and PG side at different viewing angles (Scale bar of digital photos: 0.5 cm). G,H) FESEM images of the PC side and PG side (Scale bar: 500 nm). I) The scheme of the USAXS test and J) 2D USAXS patterns of JSCMs prepared by PEG-800 and PEG-1000 at different angles ($\theta = 0°$: JSCM is positioned perpendicular to the X-ray beam; $\theta = +85°$: JSCM is rotated 85° clockwise; $\theta = -95°$: JSCM is rotated 95° anticlockwise).

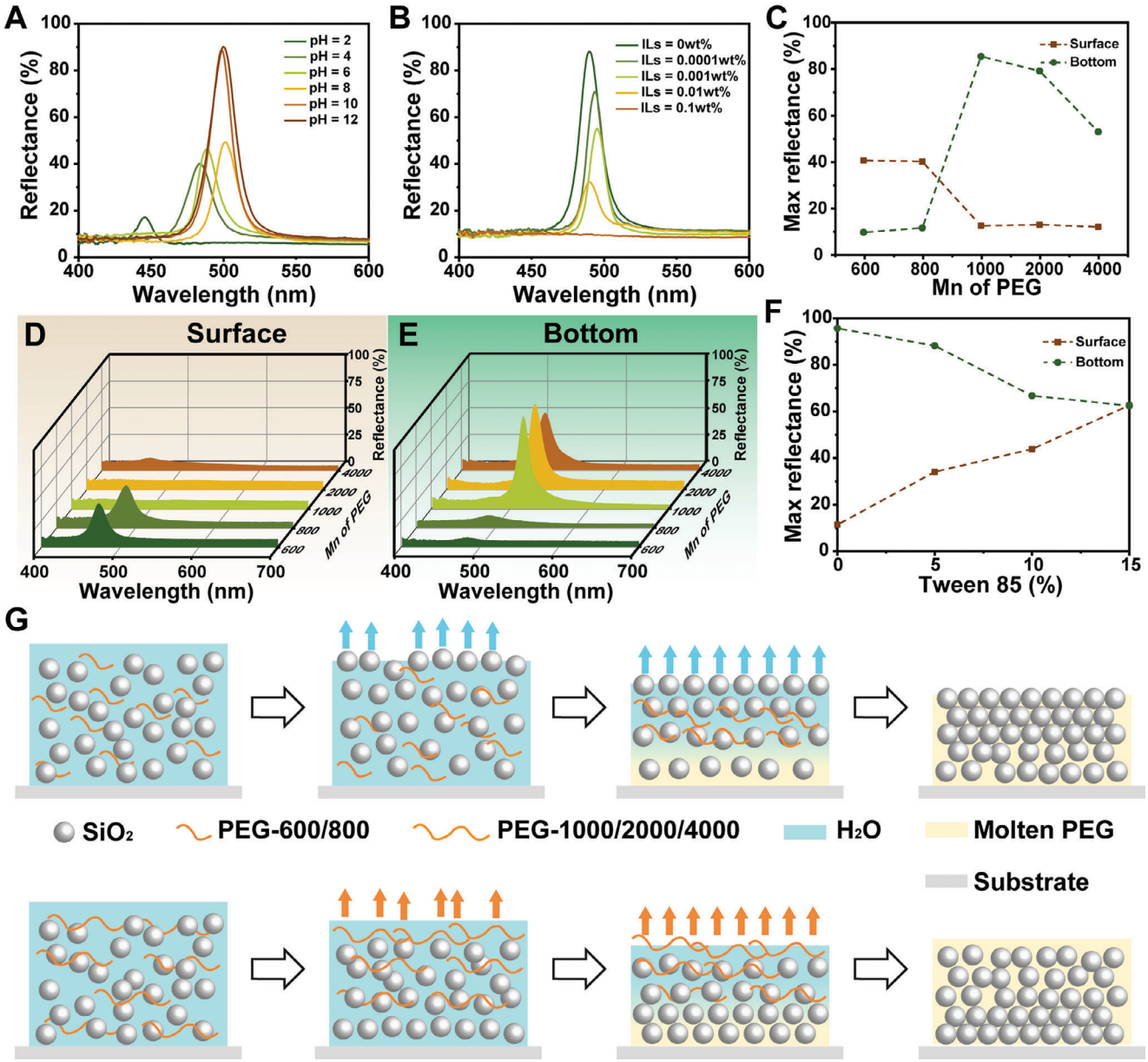

Figure 2. Exploration of the forming mechanism of JSCMs. A) Reflection spectra of PC side of JSCMs prepared at different pH and B) by adding different amounts of ionic liquid ($EMImNTf_2$). C) The max spectral reflectance, D) surface, and E) bottom reflection spectra of JSCMs prepared with PEG of different molecular weights. F) Variations of the max spectral reflectance of JSCMs prepared with PEG-1000 after adding different contents of Tween-85. G) Schematic diagram of the assembly mechanism. The blue and orange arrows respectively indicate that the SiO_2 nanoparticles or PEG have the tendency to move upward due to surface tension.

solution.[14] In polar solvents like water, the silanol groups on SiO_2 surfaces can dissociate to release H^+, making the nanoparticles have negative charges, as confirmed by zeta potential measurements. This mechanism can be verified by adjusting the system's pH and ionic strength. As the pH decreases, the negative charge on the silica surface is gradually neutralized, resulting in a decrease in reflection intensity and a broadening of the peak width on the PC side (**Figure** 2A). Another factor affecting optical intensity under acidic conditions is the enhanced hydrogen bonding between silanol groups and PEG, which restricts the movement and assembly of silica nanoparticles during water evaporation. Further evidence comes from altering the range of electrostatic forces (Debye length, λ_D).[15]

$$\lambda_D = \left(\varepsilon k_B T / 2000 N_A e^2 I\right)^{1/2} \quad (1)$$

where ε is the dielectric constant, k_B is Boltzmann's constant, T is the absolute temperature, N_A is Avogadro's number, e is the elementary charge, and I is the ionic strength. The Debye length is inversely related to ionic strength, as the concentration of ionic liquid ($EMImNTf_2$) increases, the reflection intensity

significantly decreases (Figure 2B), indicating that the ionic liquid effectively weakens the electrostatic repulsion between SiO_2 nanoparticles. Transmission spectra change under varying pH and ionic liquid concentrations show similar trends (Figure S9, Supporting Information), confirming that electrostatic interactions between the nanoparticles are crucial for forming a well-ordered arrangement.

The formation of the coexisting long-range ordered and short-range ordered arrangement of SiO_2 nanoparticles is achieved through rapid water evaporation. Typically, extending the evaporation time (up to a hundred hours) can yield a perfectly ordered array of silica nanoparticles, similar to an annealing process.[16] In this system, rapid evaporation at 80 °C (assembly time ≤ 10 min) allows only part of the silica nanoparticles to form a highly ordered structure (Figure S10, Supporting Information), while the rest nanoparticles do not have enough time to achieve a fully ordered arrangement. As a result, a structure with both PC and PG domains is obtained (Figure 1J, $\theta = 0°$).

By varying the molecular weight of PEG in the system, we can precisely control the spatial position of the PC and PG domains within the material. This is due to the competition between PEG and silica nanoparticles to minimize interfacial surface tension during solvent evaporation. We observe optical property changes on the surface (exposed to air) and bottom (contact with the glass dish) of the material when using PEGs with different molecular weights (Figure 2C–E). Using PEG-600 and PEG-800, the surface sides show significantly higher reflection intensity than the bottom (Figure 2C), along with a typical PC reflection peak (Figure 2D). In contrast, using PEG-1000, 2000, and 4000, the bottom sides exhibit much higher reflection intensity and distinct reflection peaks (Figure 2E). Using different substrates, such as plastic or aluminum foil, shows that the materials assembled with PEG-800 and PEG-1000 retain similar optical properties, indicating that the substrates do not influence the assembly behavior of the SiO_2 nanoparticles (Figure S11, Supporting Information). Meanwhile, with the increase of PEG molecular weight, the reflection peak of JSCMs increases initially and decreases subsequently. This trend may be influenced by the surface tension and viscosity, when the molecular weight of PEG is too low, the high surface tension and low viscosity is not good for the formation of PC structure, however, when the molecular weight is excessively high, chain segment entanglement (high viscosity) interferes with the spatial arrangement of the SiO_2 nanoparticles. The optimal assembly and arrangement of SiO_2 nanoparticles are achieved with the PEG-1000.

Using the pendant drop method, we measured the surface tension of water dispersion of PEG-800, SiO_2 nanoparticles, and PEG-1000 with the same concentration in the assembling process. The results show that the surface tension of the silica nanoparticle dispersion is lower than that of PEG-800 but higher than PEG-1000 (Figure S12, Supporting Information). Generally, within a certain molecular weight range, an increase in PEG molecular weight (600–4000) effectively reduces the surface tension of the aqueous system.[17] We propose that when PEG has a relatively low molecular weight and is more hydrophilic (e.g., PEG-600, 800), the silica nanoparticles are more effective to reduce the surface tension and thus tend to accumulate at the surface, where they begin self-assembling into a highly ordered structure. Meanwhile, due to the rapid evaporation of water, nanoparticles in other regions of the system do not have sufficient time to achieve a highly ordered arrangement, resulting in short-range ordered structures. As the PEG molecular weight increases, its hydrophobicity also increases (e.g., PEG-1000, 2000, and 4000), making PEG more likely to accumulate at the interface. This causes the silica nanoparticles to concentrate at the bottom, where they self-assemble into a long-range ordered photonic crystal structure, while short-range ordered photonic glass structure forms in other regions of the material (Figure 2G).

Based on this mechanism, adding surfactant with low-surface energy will greatly influence the formation of the JSCM. Then, Tween-85 is added into the above system, which will cause Tween-85 to preferentially occupy the water/air interface.[18] As a result, the spatial distribution of silica nanoparticles and PEG during water evaporation becomes non-preferential. For example, in the PEG-1000 system, after water evaporation, the reflection intensities of the photonic crystal peaks on both surface and bottom showed a tendency to get closer (Figure 2F; Figure S13, Supporting Information), this effect is more obvious with higher tween-85 concentrations.

2.3. Preparation of Bright Polychromatic JSCMs

To create a color palette of JSCMs, we first focus on optimizing the optical performance of the PC side. By analyzing the reflection peaks of JSCMs prepared with PEG of different molecular weights, it is found that the JSCM made with PEG-1000 has the maximum reflection intensity and the narrowest FWHM (Figure 2C–E). Subsequently, four differently colored JSCMs are prepared by adjusting the volume fractions of silica and PEG-1000 (**Figure 3**A; Figure S14, Supporting Information). The results showed that the interparticle distance decreased with the increase of the volume fraction of silica nanoparticles, leading to a tighter arrangement and a blue shift in the reflection peaks. For the different volume fraction samples, the JSCM with a 50% volume fraction of silica nanoparticles exhibits the maximum reflection intensity and the narrower FWHM (Figure S15, Supporting Information). This phenomenon could be attributed to the gradual increase in the volume fraction of SiO_2 nanoparticles, which lead to a closer arrangement and stronger electrostatic repulsion between them. Consequently, the arrangement of SiO_2 nanoparticles becomes more orderly, resulting in a gradual decrease in the half-peak width. However, when the volume fraction exceeds 50%, the excess of SiO_2 nanoparticles makes their movement limited and leads to the degradation of the reflection peak.

Next, we prepared six different sizes of SiO_2 nanoparticles, their TEM images and particle size distributions proved their uniformity (Figure S16, Supporting Information). The hydrated particle sizes and zeta potentials are shown in Figure 3B. All prepared silica nanoparticles have uniform sizes and good dispersibility with zeta potentials ≈−50 mV, which provides a solid foundation for their electrostatic self-assembly into JSCMs. Then these SiO_2 nanoparticles are used to prepare six differently colored JSCMs with a 50% volume fraction of silica in PEG-1000. The digital photos and microscope images of the PC sides

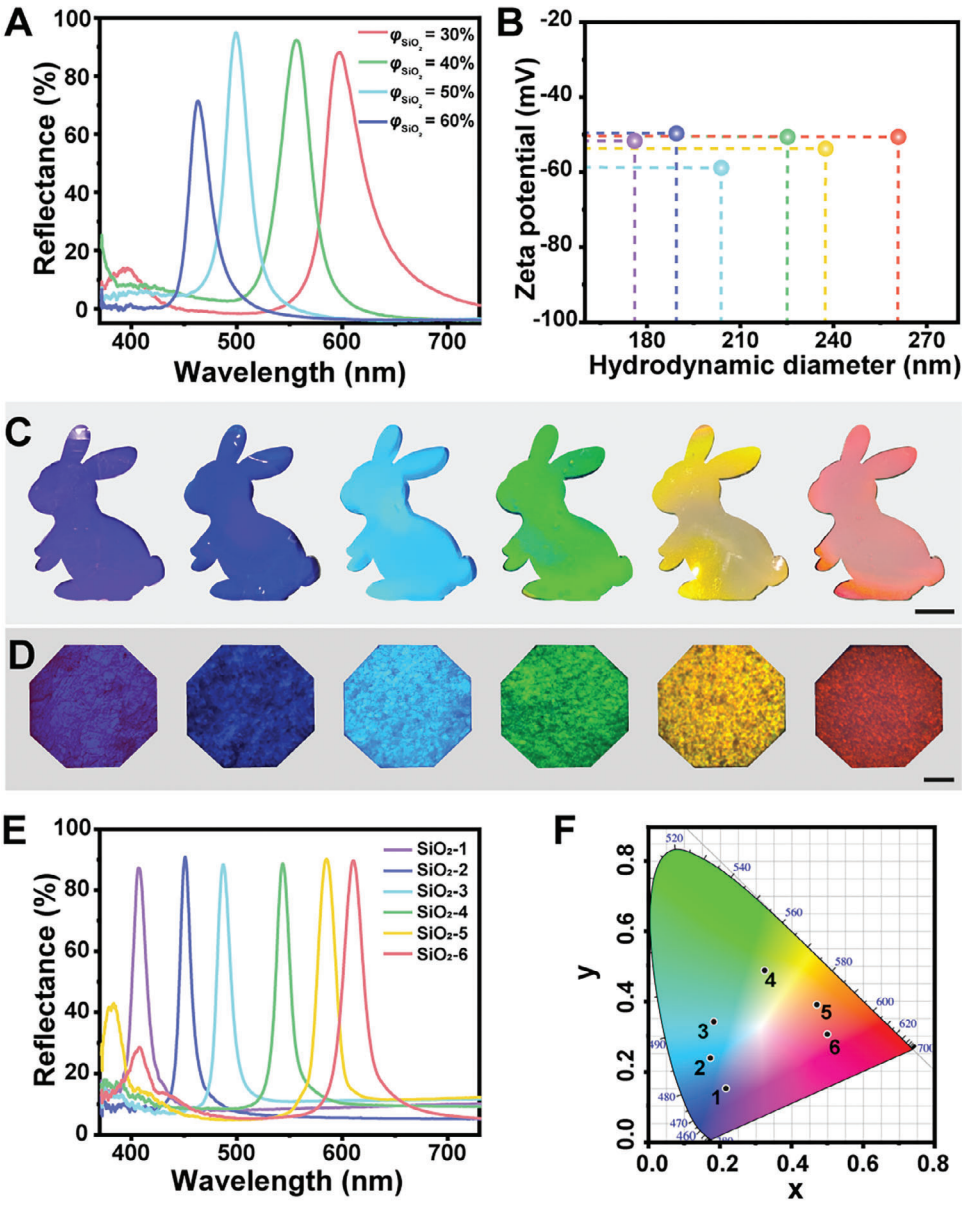

Figure 3. Preparation and characterization of polychromatic JSCMs. A) Reflection spectra of the PC side of polychromatic JSCMs prepared with PEG-1000 and different volume fractions of SiO_2 nanoparticles. B) DLS and zeta potential characterization of SiO_2 with different sizes. C) Digital photos (scale bar: 0.5 cm), D) microscope photos (scale bar: 10 μm), E) reflection spectra, and F) CIE coordinate diagram of the PC side of polychromatic JSCMs prepared with different sizes of SiO_2 nanoparticles.

display vibrant structural colors (Figure 3C,D). The corresponding reflectance spectra show reflectance close to 90% and achieve a span of 413–605 nm (Figure 3E). As shown in Figure 3F, the colors of these JSCMs cover the entire visible range in the CIE diagram.

2.4. Multi-Level Optical Encryption and Anti-Counterfeiting of JSCMs

To develop a JSCM system with multi-optical signals, the fluorescein isothiocyanate (FITC), which absorbs light at wavelengths between 400 and 500 nm (Figure S17A, Supporting Information), is incorporated as the fluorescent probe. When FITC is added into JSCMs prepared with PEG-800 and PEG-1000, the experimental results demonstrate that FITC does not significantly affect the assembly of the SiO_2 nanoparticles, with the reflection spectra remaining stable (Figure S18, Supporting Information). However, there is a notable difference in fluorescence intensity between the surface and bottom sides. In the PEG-800 system, the surface fluorescence is 2.1 times higher than that of the bottom, whereas in the PEG-1000 system, the bottom-side fluorescence is 1.1 times higher than that of the surface. All indicate that the PC side exhibits a higher

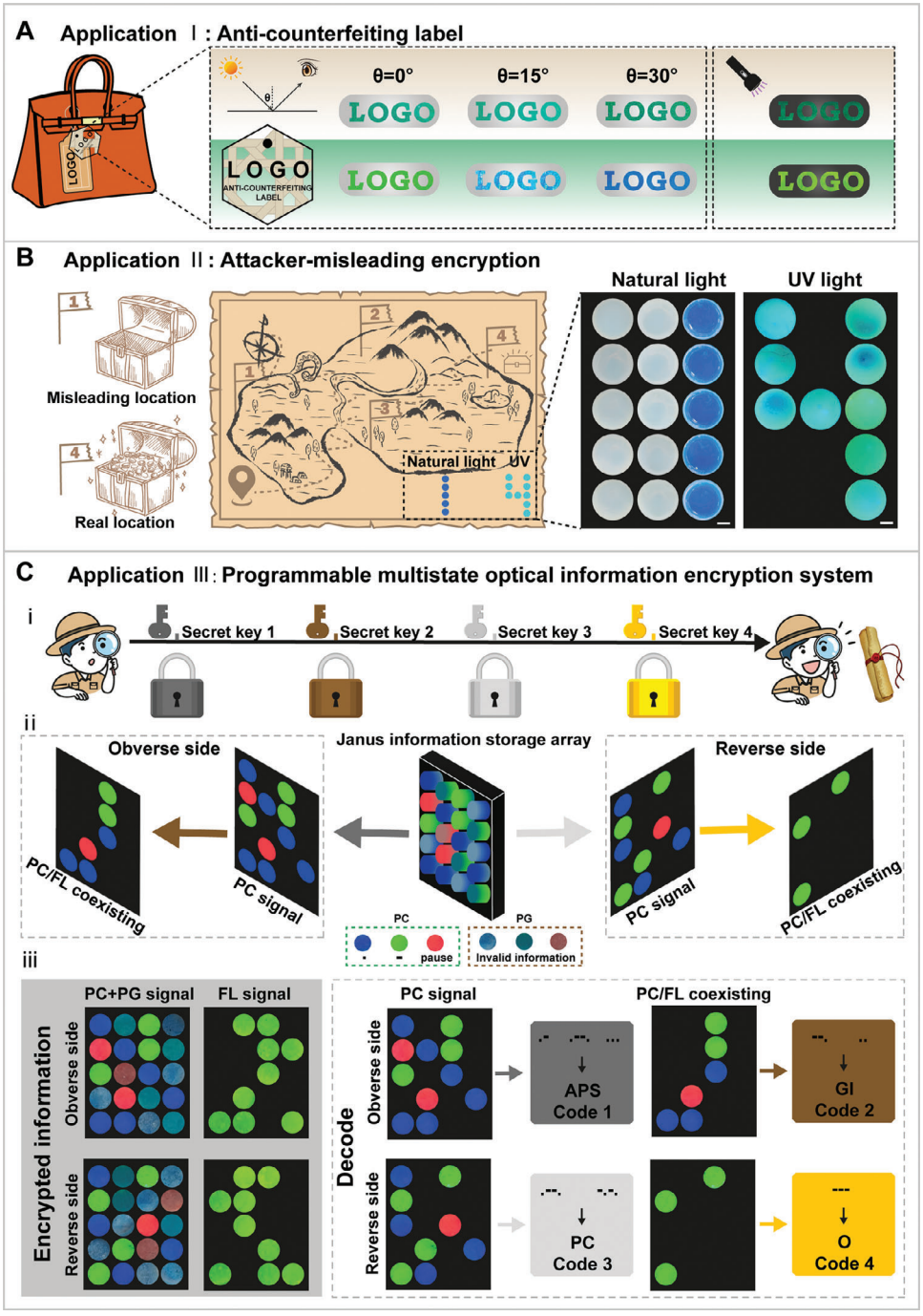

Figure 4. Applications of JSCMs with multistage optical signals. A) The anti-counterfeiting effect of the JSCM label under natural light and UV light (the top line is the PG side and the bottom line is the PC side). B) Attacker-misleading encryption: The misleading information is displayed by structural color and the correct information is displayed after UV light irradiation (Scale bar: 0.5 cm, FITC concentration: 0.5 wt.%). C) Programmable multistate optical information encryption system: i) Multi-level information encryption diagram; ii) Schematic diagram of the multiple signals outputted by the Janus information storage array; iii) Display of multi-level information encryption and decoding based on Morse code.

fluorescence intensity compared to the PG side. This discrepancy arises from the bandgap difference between the PC and PG. The reflection peak of the PC side in the PEG-800 system is at 475 nm, which more closely matches the excitation wavelength of FITC, resulting in a stronger fluorescence enhancement. A control group (FITC+PEG 1000) was prepared and showed no significant difference in fluorescence intensity between the surface and bottom sides (Figure S17B, Supporting Information), indicating that FITC is evenly distributed in PEG after solvent evaporation.

By integrating structural color and fluorescence, as well as leveraging the Janus structure of the material to generate multi-level optical signals, JSCMs can be effectively applied in anti-counterfeiting and information encryption. As shown in **Figure** 4A, a brand logo is created on the label using green JSCM doped with black pigment and the fluorescent dye FITC. This label provides dual anti-counterfeiting functionality. The first level of authentication is visible under natural light, where different viewing angles cause structural color changes on both sides of the label. One side appears bright colors (PC side, bottom line), shifting from green to blue when viewed from 0° to 30°, while the other side (PG side, top line) remains a dull green with minimal visible color change. The second level of authentication is activated under UV light, revealing a green fluorescent logo emitted by FITC, and a higher fluorescence intensity is shown on the PC side of the label.

To further demonstrate the potential of JSCMs in multi-level information encryption, we design a digital dot matrix display system based on blue JSCMs doped with the green fluorescent dye FITC (Figure 4B). This system conveys misleading information through structural color while displaying the correct information via fluorescence. In a treasure map application, the number "1" is shown under natural light as misleading structural color information, while the correct treasure location, represented by the number "4" is revealed only under UV light. This design showcases the encrypted misleading information function of JSCMs, where only by unlocking the correct location code can the treasure hunter be guided to the right location.

In addition, a programmable multistate optical information encryption system was developed for multi-level information storage (Figure 4C). This system is based on the color differences between the PC and PG sides of JSCMs assisted by deep encryption of fluorescent information, creating a four-level decoding process. It uses the different bright PC side colors of JSCMs as valid information, while the dull PG side colors serve as invalid information, significantly enhancing information security. By arranging red, blue, and green JSCM dots, a 4 × 6 double-sided Janus information storage array was construct, where decryption is performed using Morse code. The bright blue and green colors of the PC side represent the dots and dashes in Morse code, respectively, while red indicates the end of a piece of information.

As shown in Figure 4C, the system's first-level password is displayed through the PC signal in the array's obverse side, revealing "APS". The second-level password is indicated by the PC signal coexisting with the fluorescent signal in the array's obverse side, showing "GI". The third-level password is displayed by the PC signal in the array's reverse side, revealing "PC", while the fourth-level password is indicated by the PG signal coexisting with the fluorescent signal in the array's reverse side, showing "O". After decoding all four levels, the final information is revealed.

This programmable multistate optical encryption information system offers protection for critical data through the heterogenous and asymmetric structures of JSCMs, which also can customize multi-level encryption. The system significantly enhances information storage capacity, with each level following specific coding rules to conceal multiple levels of sensitive data. The flexibility of the coding rules, combined with the diversity of output signals, greatly reduces the risk of theft and information leakage. Therefore, this programmable optical encryption system provides a high level of security. These applications also demonstrate the immense potential of JSCMs in anti-counterfeiting and contribute to advancements in the field.

3. Conclusion

Inspired by the unique front and back color differences in peacock feathers caused by structural variations, we design and develop a new kind of Janus structural color material, which can achieve different micro-nano structures and structural colors on the obverse side and reverse side, respectively. Using a simple one-step process, we utilize the competition between PEG and silica nanoparticles for minimizing surface tension during solvent evaporation, resulting in a structure where photonic crystal and photonic glass coexist. This approach enables precise control over the formation locations of the long-range ordered and short-range ordered domains. Based on the distinct brightness, angle-dependent color shift, and fluorescence enhancement of the JSCMs, we successfully designed a diverse, cost-effective, and unique anti-counterfeiting label. Finally, a programmable multi-level optical information encryption and decoding system based on the JSCM label was demonstrated. However, the JSCMs have poor performance in terms of anti-friction and free-standing properties due to the limitations of the material itself. It is hoped that the subsequent work can gradually solve these defects and maintain the structural properties of the material through better curing methods. All-in-all, inspired by peacock feathers, we offer a new technology that is easy to make, flexible, and secure with multilevel optical encryption and anti-counterfeiting.

Supporting Information

Supporting Information is available from the Wiley Online Library or from the author.

Acknowledgements

L.C. and H.L. contributed equally to this work. This work was financially supported by the National Natural Science Foundation of China (Grant Nos. 52131308, 52373131), MOST (2022YFA1203002), Key research and development project of Guangdong Province (Grant No. 2020B010190003), and the Shanghai Sailing Program (Grant Nos. 24YF2702000). The authors are grateful to the time-resolved USAXS Beamline BL10U1 at SSRF (Shanghai Synchrotron Radiation Facility, China) for providing the beam time.

Conflict of Interest

The authors declare no conflict of interest.

Data Availability Statement

The data that support the findings of this study are available from the corresponding author upon reasonable request.

Keywords

anti-counterfeiting, Janus structure, optical encryption, photonic crystal, photonic glass

Received: January 1, 2025
Revised: February 14, 2025
Published online:

[1] S. Kinoshita, S. Yoshioka, J. Miyazaki, *Rep. Prog. Phys.* **2008**, *71*, 076401.
[2] a) W. D. Bancroft, *Nature* **1923**, *2807*, 243; b) K. Yu, T. Fan, S. Lou, D. Zhang, *Prog. Mater. Sci.* **2013**, *58*, 825; c) Y. Fu, C. A. Tippets, E. U. Donev, R. Lopez, *Wiley Interdiscip. Rev.:Nanomed. Nanobiotechnol.* **2016**, *8*, 758.
[3] Y. Zhan, Y. Wang, Q. Cheng, C. Li, K. Li, H. Li, J. Peng, B. Lu, Y. Wang, Y. Song, L. Jiang, M. Li, *Angew. Chem., Int. Ed.* **2019**, *58*, 16456.
[4] a) X. Lai, J. Peng, Q. Cheng, A. P. Tomsia, G. Zhao, L. Liu, G. Zou, Y. Song, L. Jiang, M. Li, *Angew. Chem., Int. Ed.* **2021**, *60*, 14307; b) H. Huang, H. Li, J. Yin, K. Gu, J. Guo, C. Wang, *Adv. Mater.* **2023**, *35*, 2211117; c) H. Yuan, Z. Zhong, B. Zhang, *Photonics Res.* **2024**, *12*, 356.
[5] a) Z. Cai, Z. Li, S. Ravaine, M. He, Y. Song, Y. Yin, H. Zheng, J. Teng, A. Zhang, *Chem. Soc. Rev.* **2021**, *50*, 5898; b) Q. Chen, C. Ouyang, Z. Xie, C. Xu, Z. Wu, J. Min, Y. Liu, D. Luo, W. Hu, *Laser Photonics Rev.* **2024**, 2401635, https://doi.org/10.1002/lpor.202401635. c) C. Ouyang, Q. M. Chen, Z. Y. Xie, C. T. Xu, Q. G. Wang, Z. G. Zheng, D. Luo, Y. Q. Lu, W. Hu, *Adv. Opt. Mater.* **2024**, 2402844, https://doi.org/10.1002/adom.202402844.
[6] a) S. Kinoshita, S. Yoshioka, K. Kawagoe, *Proc. Biol. Sci.* **2002**, *269*, 1417; b) S. Vignolini, P. J. Rudall, A. V. Rowland, A. Reed, E. Moyroud, R. B. Faden, J. J. Baumberg, B. J. Glover, U. Steiner, *Proc. Natl. Acad. Sci. U. S. A.* **2012**, *109*, 15712.
[7] J. Zi, X. Yu, Y. Li, X. Hu, C. Xu, X. Wang, X. Liu, R. Fu, *Proc. Natl. Acad. Sci. U. S. A.* **2003**, *100*, 12576.
[8] a) E. Yablonovitch, *Phys. Rev. Lett.* **1987**, *58*, 2059; b) S. John, *Phys. Rev. Lett.* **1987**, *58*, 2486.
[9] a) Z. Li, T. Ma, S. Li, W. Gu, L. Lu, H. Yang, Y. Dai, R. Wang, *ACS Nano* **2022**, *16*, 11473; b) J. Sun, Y. Zheng, J. Chen, W. Hong, *Chem. Eng. J.* **2024**, *489*, 151131.
[10] H. Ragelle, M. W. Tibbitt, S. Y. Wu, M. A. Castillo, G. Z. Cheng, S. P. Gangadharan, D. G. Anderson, M. J. Cima, R. Langer, *Nat. Commun.* **2018**, *9*, 1184.
[11] a) X. Li, L. Chen, Y. Ma, D. Weng, Z. Li, L. Song, X. Zhang, G. Yu, J. Wang, *Adv. Funct. Mater.* **2022**, *32*, 2205462; b) J. Liao, C. Majidi, M. Sitti, *Adv. Mater.* **2023**, *36*, 2300560; c) J. Shen, J. Wu, M. Wang, P. Dong, J. Xu, X. Li, X. Zhang, J. Yuan, X. Wang, M. Ye, R. Vajtai, J. Lou, P. M. Ajayan, *Small* **2016**, *12*, 2741.
[12] H. Li, Z. Fu, X. Yu, Y. Song, K. Qiu, S. Lu, *Chem. Eng. J.* **2024**, *493*, 152635.
[13] H. Noh, S. F. Liew, V. Saranathan, S. G. Mochrie, R. O. Prum, E. R. Dufresne, H. Cao, *Adv. Mater.* **2010**, *22*, 2871.
[14] G. Bao, W. Yu, Q. Fu, J. Ge, *Adv. Opt. Mater.* **2022**, *10*, 2201188.
[15] Y. Hu, D. Yang, D. Ma, S. Huang, *Chem. Eng. J.* **2022**, *429*, 132342.
[16] M. Li, Z. Li, Q. Lyu, B. Peng, R. Zhong, M. Zhao, B. Xiong, G. Yi, L. Zhang, J. Zhu, *Macromolecules* **2022**, *55*, 8345.
[17] M. Yen, T. C. Yeh, *J. Polym. Res.* **1997**, *4*, 253.
[18] S. Cai, C. Pan, J. Li, D. Zhang, *J. Energy Storage* **2024**, *79*, 110136.